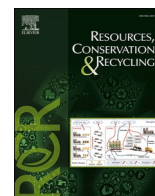




Contents lists available at ScienceDirect

## Resources, Conservation &amp; Recycling

journal homepage: [www.elsevier.com/locate/resconrec](http://www.elsevier.com/locate/resconrec)

## Sorting plastics waste for a circular economy: Perspectives for lanthanide luminescent markers

Ian A. Howard<sup>a,b,\*</sup>, Dmitry Busko<sup>a</sup>, Guojun Gao<sup>c</sup>, Pascal Wendler<sup>c</sup>, Eduard Madirov<sup>a</sup>, Andrey Turshatov<sup>a</sup>, Jochen Moesslein<sup>c</sup>, Bryce S. Richards<sup>a,b,\*</sup>

<sup>a</sup> Institute of Microstructure Technology, Karlsruhe Institute of Technology, Hermann-von-Helmholtz-Platz 1, 76344, Eggenstein-Leopoldshafen, Germany

<sup>b</sup> Light Technology Institute, Karlsruhe Institute of Technology, Engesserstrasse 13, 76131, Karlsruhe, Germany

<sup>c</sup> Polysecure GmbH, St. Georgener Str. 19, 79111, Freiburg, Germany

### ARTICLE INFO

#### Keywords:

Plastic waste  
Luminescent marker  
NIR luminescence  
Tracer-based sorting  
Multi-class classification

### ABSTRACT

Improved sorting of plastic waste will be needed to increase the circularity of the plastics industry, irrespective of innovations in recycling technologies. The variety of recycling processes available in the future will not alleviate the need for sorting. Rather, nuanced sorting will be necessary to distribute waste streams into tailored feedstocks within an ecosystem comprising of various mechanical and chemical processes. A system for marking plastics with codes that are invisible to consumers, but readily apparent to sorting machines is of interest to enable such nuanced sorting. Luminescent lanthanide markers offer a promising solution, adding unique spectral signatures in the visible and near-infrared (NIR) to allow innovative new sorting options. Currently, 21 codes can be created using mixtures of three upconversion markers when excited with a 978 nm laser and measured with >99% accuracy. This range can be expanded with further NIR emitting markers, whose emission can be obtained at the same time as characterizing the NIR reflectance of plastics.

## 1. Introduction

### 1.1. Plastics recycling landscape

The motivations to increase the circularity of the plastics industry are immediately understandable. Firstly, producing plastics from non-renewable feedstocks leads to resource depletion. Sustainable access to this important material class must ultimately be achieved. Secondly, the plastics industry is responsible for 4.5% of total greenhouse gas emissions (Stegmann et al., 2022). However, by adopting circular recycling practices and increasing the use of biomass in feedstocks, the sector could ultimately become carbon neutral or even a net carbon sink (Stegmann et al., 2022). Thirdly, the ecological damage caused by improper disposal of plastics waste into ecosystems must be minimised (Gontard et al., 2022; Law and Narayan, 2021). In recognition of these considerations, legislative efforts aimed at accelerating the transition to a circular plastic economy are increasing (GAIA, 2021; US Government, 2022; European Parliament, 2023), and serious commercial investments in innovative chemical recycling pilot-lines and plants being made (Niessner, 2022).

This article will focus on circularity in the subspace of plastic packaging waste. Due to the short product lifetime of plastic packaging, the amount of plastic packaging waste collected tracks the amount of plastic packaging produced with a negligible time lag. This, alongside the significant fraction of total plastics production that packaging accounts for (namely 40%) (European Parliament, 2023), makes plastic packaging a good initial target for establishing circularity. As a concrete example, of the 29 million tonnes of plastics post-consumer waste collected in the European Union (EU) in 2020, only 35% was recycled, with the remaining fraction either being burnt for energy recovery (42%) or placed into landfills (23%) (Plastics Europe, 2020). The EU's goal is to recycle 55% of plastic packaging waste by 2030 (European Commission, 2017). In contrast, the in-use stock of construction plastics, i.e., plastics incorporated in buildings, continues to grow rapidly and will ultimately need to be recycled in the future – e.g., a predicted 5 billion tonnes of construction materials will comprise more than 50% of in-use plastic by 2100 (Stegmann et al., 2022). The experience gained in circularizing the shorter in-use packaging will thus contribute to the recycling of these other future waste streams.

A range of recycling technologies are established and under

\* Corresponding authors.

E-mail addresses: [ian.howard@kit.edu](mailto:ian.howard@kit.edu) (I.A. Howard), [bryce.richards@kit.edu](mailto:bryce.richards@kit.edu) (B.S. Richards).

<https://doi.org/10.1016/j.resconrec.2024.107557>

Received 16 November 2023; Received in revised form 6 February 2024; Accepted 10 March 2024

Available online 19 March 2024

0921-3449/© 2024 The Author(s). Published by Elsevier B.V. This is an open access article under the CC BY license (<http://creativecommons.org/licenses/by/4.0/>).

development (Garcia and Robertson, 2017; Mangold and von Vacano, 2022). Mechanical recycling can involve ‘simply’ the re-extrusion and regranulation of sorted flakes of thermoplastics (plus some additives to improve recyclate quality), or the dissolution of the polymer chains, their cleaning, and reprecipitation before regranulation (solvent-based recycling) (Schyns and Shaver, 2021). Chemical recycling can involve the pyrolysis of hydrocarbon – those made of only carbon and hydrogen atoms, e.g., the polyolefins of polypropylene (PP) and polyethylene (PE) – to produce pyrolysis oil (Anuar Sharuddin et al., 2016). Pyrolysis oil can then be introduced into a steam cracker to offset some portion of virgin naphtha. The monomers produced from the steam cracker can then be polymerised to create virgin-equivalent plastics. This is so-called mass-balance recycling wherein the recycled plastics produced may not actually contain the carbon atoms from the plastic waste; but these are in some chemical products and therefore the waste plastic has offset virgin hydrocarbon consumption. Another expanding method of chemical recycling is remonomerisation of the waste plastic, breaking the polymer chains into their building blocks, such that these building blocks can be again polymerised into materials of virgin quality (Coates and Getzler, 2020; Jehanno et al., 2022). Depending on the input waste stream and the desired use of the output recyclate, each of these recycling technologies has a role to play in the transition towards a more circular plastics industry. A recent article Uekert et al. gives an excellent overview of the roles that each of the recycling technologies can play based on the available input stream and desired output stream (Uekert et al., 2023).

Realistically, it is vanishingly unlikely that there will be a single plastics recycling process that offers a simple road to circularity and eliminates the need for sorting. Even though innovative chemical recycling approaches can, in some cases, be made robust to impure inputs such as mixed textiles or multilayer packaging (Nicholson et al., 2022), the most attractive option will be to sort waste streams into feedstocks tailored to maximise the efficiency and throughput of specific recycling processes. Furthermore, it is highly likely that mechanical recycling will remain the most energetically favourable recycling process. Mechanical recycling has the disadvantage that the polymer chains are altered during the process meaning that it can only be repeated a finite number of times before the material properties degrade, unless a portion of e.g. 30% non-degraded material is blended to well sorted waste material. Thus, an effective and nuanced sorting system will be a central component of a circular plastics industry. An efficient system might well

be one that sorts plastic items by polymer, by certain extra characteristics (e.g., food-grade), and by how many times the plastic in the object has been mechanically recycled. This would allow objects to be efficiently mechanically recycled as many times as possible before going through a chemical recycling process to fully refresh the material properties.

This article discusses the perspectives for how upconverting and down-shifting luminescent inorganic microparticles can be mixed into plastics to introduce emission lines in the visible and near-infrared (NIR) that are readily detectable with existing detection systems such as InGaAs-based spectrometers or hyperspectral cameras. Based on the emission from these lanthanide luminescent markers (that do not alter the visible appearance of the plastics), codes can be made that could be read out as the objects move through a measuring station on a conveyor belt. It is considered how a system, like that shown in Fig. 1, could be realised based on the measurement of such a code plus an identification of the plastic type based on its NIR reflectance (a technique currently used in state-of-the-art sorting facilities). Initial investigations are shown that demonstrate at least 21 codes can be differentiated using mixtures of lanthanide luminescent upconversion markers in white micron-scale materials. How the number of differentiable codes could be increased by material and detector developments is discussed. Also, it is shown that NIR markers can be made that give sufficient signal in the NIR to allow them to be identified at the same time as the diffuse reflectance of the polymer is classified.

## 1.2. Sorting figures-of-merit

Sorting entails deciding to which of various output streams each object in the input stream should be assigned. The performance of a sorting system can be quantified by looking at a confusion matrix that presents the ground truth of the weights of a waste stream placed into a sorting system and an examination of the true nature of each of the output streams from the system. A material flow analysis was performed by Picuno et al. for the inputs and outputs of an materials recovery facilities (MRF) in Germany (Picuno et al., 2021). An approximate confusion matrix can be derived from their data, where the distribution of how a plastic of a given type is mis-sorted between the ‘mixed plastic’ and other pure plastic types is estimated. Table 1 demonstrates a hypothetical case how high-density polyethylene (HDPE), PP, and polyethylene terephthalate (PET) packaging waste – all of which can be

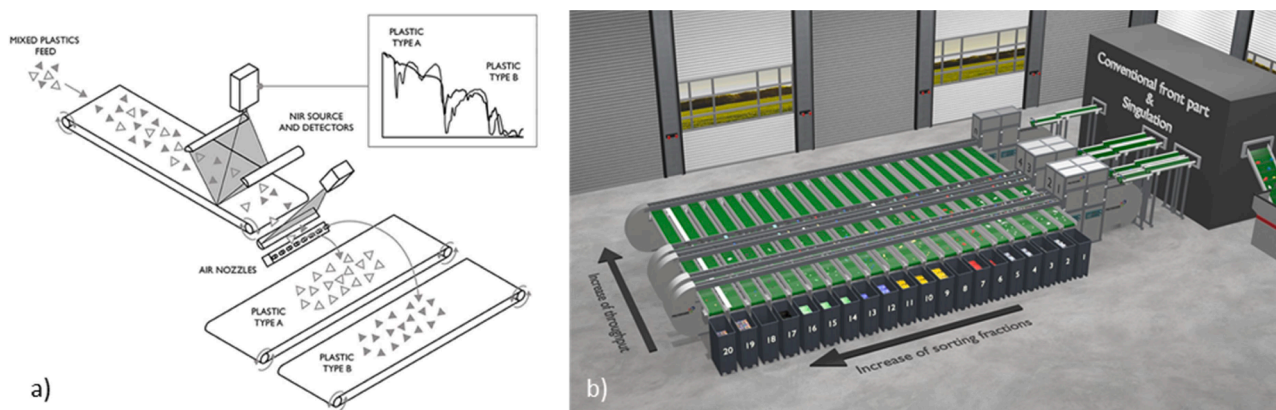


**Fig. 1.** a) Typical present-day NIR sorter showing measurement of NIR reflectance and physical sorting based on actuated air nozzles changing the flight path of classified objects (reproduced from (Taneepanichskul et al., 2022)). Sorting is achieved by a series of such characterisation stations in series and binary decisions. The throughput per metre bandwidth is high, but each sorting fraction requires a new sorting step making the total system expensive when sorting into more fractions is desired. b) Example of a next-generation sorting system (Moesslein et al., 2023) wherein objects are placed one at a time onto a tray conveyor, which then passes through a detection unit. This unit accurately identifies each object before depositing it directly into its designated endpoint. Unlike the typical pneumatic ejection method, which often struggles with accuracy, especially when dealing with overlapping objects, the system’s ability to handle separated objects greatly increases efficiency and accuracy. Macroscopic objects that have been singulated can be sorted into multiple output fractions following a single characterization process. To enhance throughput, parallel characterization lines are employed. This approach not only allows for a high number of sorting fractions from a single stage but also significantly boosts throughput through parallelization.

**Table 1**

Confusion matrix showing typical inputs to a German sorting facility for the main three types of rigid plastic packaging waste, the sorting output is hypothetical (given to explain how sorting figures of merit are derived), but chosen to be consistent with the data found in reference (Picuno et al., 2021).

Sorted True	PP	PET	HDPE	Mixed-plastic	Input
PP Food-Grade	15.6	1.3	1.3	7.8	26
PP Non-Food-Grade	10.2	0.5	1.2	5.1	17
PET Food-Grade	0.7	10.2	0.2	6.0	17
PET Non-Food-Grade	0.5	10.2	0.7	5.6	17
HDPE Food-Grade	0.2	0.0	0.6	1.2	2
HDPE Non-Food-Grade	2.1	0.0	6.3	12.6	21
Sorted Output	29.3	22.2	10.2	38.3	

food-grade or not – have been sorted by a technology into four output bins (one bin for each type and an ‘mixed-plastic’ bin in which items are placed when no decision could be reached). From such a confusion matrix, the key figures-of-merit (FoMs) of the sorting system can be understood. On a global system level, the most important FoMs are accuracy and throughput. The accuracy is the total correctly sorted mass (sum of the entries where the input polymer is sorted into the correct output stream) divided by the sum of the total mass to sort, whereas the throughput is the mass of material sorted per time, usually given in tonnes per hour (with throughputs of several tonnes per hour desired and realisable for current applications). In this hypothetical example, the accuracy of the sorting system is 53%. Optimizing accuracy guarantees that the maximum volume of feedstocks with stable profiles can be created from waste streams. Optimizing throughput means that this can be done with a minimum number of machines (increasing the economic viability).

Furthermore, the purity is a key FOM for recyclers purchasing the sorted output of a given material. Purity (also called precision or positive predictive value) is the percentage of the correct material in a given output stream. In the hypothetical example above, the purity of the sorted PET would be 92%. A high purity can come at the cost of decreasing the yield (also called sensitivity or true positive rate), which is the percentage of the total mass of a given material that is correctly identified. This is a trade-off as the decreased yield also decreases the amount of material the MRF can sell. Furthermore, it should be noted that the MRF cannot currently separate food from non-food grade plastics. Hence approaches to add additional waste streams and separate the higher value food-grade packaging from non-food grade packaging would also be attractive financially and in terms of enabling true circularity. As the purity and yield for each material approach 100%, so too does the accuracy. Although accuracy is a key FoM to maximise, often the FoM quoted is the more easily measured recovery, defined as the total mass output in the sorted bins (total mass minus ‘other’ bin in this case) divided by the total mass. Based on the recovery and a mass-weighted average of the purity (if available), a system accuracy can be estimated.

The accuracy of a sorting system is determined by two processes. Firstly, the correctness of the classification of an object by the sensing system and classification algorithm, and secondly on the effect of the actuators stimulated by this classification to sort the object into a desired output stream. This manuscript lays emphasis on the former, on the adaptation of sensing systems to make nuanced and correct classifications, but challenges in accurately physically separating objects after correct classification should not be overlooked. For example, Fig. 1a schematically illustrates a typical NIR sorter wherein objects are separated into two classes using a blast of compressed air from a nozzle to modify the flight path of objects flying off a fast-moving conveyor belt (typical belt speed 3 m/s) (Taneepanichskul et al., 2022). The effectiveness of the air blasts in correctly separating the classified objects depends on belt coverage and the fraction of the material to be positively blasted out; it cannot be assumed to be 100% (Sormunen and Järvinen,

2021). In this binary sorting approach for each additional material to be sorted, another NIR sorter and ejection machine must be added in series. An alternative system using singulated macroscopic objects is illustrated in Fig. 1b. In this case, the macroscopic objects are characterised once, classified, and then the objects can be ejected into one of any number of collection bins. As the number of desired fractions of sorted material increases, so does the attractiveness of this second approach. For example, the second approach becomes more attractive if one wants to sort so specific producers get back their own materials with properties known to them, to sort food from non-food grade, or to ultimately sort items by the number of times that the plastic in the packaging has been recycled (which could possibly be tracked by the addition of lanthanide fluorescent markers).

### 1.3. Moving plastics sorting beyond state-of-the-art

The latest standard for industrial plastics sorting machines utilises NIR hyperspectral imaging to detect the NIR reflectance spectra of objects. Recent reviews have highlighted significant advancements in hardware and the ability to implement more sophisticated data reduction and classification tools (chemometric tools) in real-time, resulting in increased accuracy and the ability to separate a greater number of plastics (Neo et al., 2022; Zhao and Li, 2022). Certainly, the field has progressed from past implementations that compared only the reflectance in two NIR wavelength bands. There are also efforts to combine NIR spectroscopy with one or more of laser-induced breakdown (LIBS), Raman, or mid-IR spectroscopy, which could improve performance in certain cases (Liu et al., 2019; Neo et al., 2022; Zhao and Li, 2022).

However, separation beyond material type is important to recycle materials to the highest quality at minimum environmental cost. For this, it is of interest to develop a method to subtly mark plastic packaging with a coding system that does not disturb an objects appearance to consumers but allows the code to be easily read in a sorting facility. Two avenues of marking plastics for sorting are currently attracting attention. A few years ago, a digital watermarking process has been proposed based on a patterned modification of the polymer surface or label design. Although supposedly not visible to the human eye, this pattern can be detected by trained computer vision systems (Digimarc, 2019). A benefit of the watermark approach is that many unique codes can be generated to sort into nuanced fractions; however, the necessity to pattern the surface of an object could be a limitation – it could be difficult to apply this strategy to sorting flakes rather than whole objects. Initial semi-industrial trials on labelled objects show 95% purities in output streams at belt speeds up to 4.5 m/s (Labels and Labeling, 2022). The alternate route utilises photonic markers in the tracer-based sorting (TBS) process – luminescent materials that can be applied to the label or mixed in with the polymer (Brunner et al., 2015). A recent review introduces the concept and provides a good overview of the work in this field, including the work on organic dyes with visible emission after ultraviolet (UV) excitation (Larder and Hatton, 2023). Furthermore, Table 2 summarizes comparison of state-of-the-art technologies including NIR, LIBS, Raman, Digital watermarks and TBS. It should be noted that x-ray reflectance (XRF) – which for many years was used to detect the presence of chlorine in PVC and brominated flame retardants (Sormunen and Järvinen, 2021) – does not appear in the comparison table, with technological developments having stagnated as more novel sorting options are developed (Zhao and Li, 2022).

This article focuses on the use inorganic microparticles co-doped with ytterbium (Yb<sup>3+</sup>) and other trivalent lanthanide ions (Ln<sup>3+</sup>) to select the desired emission wavelength. It is important to acknowledge that while Ln<sup>3+</sup> are generally perceived as toxic and costly in comparison to commercial organic dyes, this perspective is not universally applicable. The integration (doping) of Ln<sup>3+</sup> into highly chemically stable crystalline materials, such as oxides, oxysulfide, molybdate and phosphates, is anticipated to significantly minimise potential interactions between Ln<sup>3+</sup> and the human or natural environment.

**Table 2**

Comparison of existing and upcoming sorting technologies. All technologies rely on the detection of an optical signal - emission in case of XRF, LIBS, Raman and TBS (using organic dyes and lanthanide (Ln) markers), and reflection in the case of NIR and digital watermarking.

Parameter Technology	Excitation	Modify packaging	Single-point measurement	Object speed	Accuracy	Purity	Refs.
NIR	Halogen lamp	No	No	3 m/s	80 - 95%	65 - 90%	(Sormunenand Järvinen, 2021); (Zhao and Li, 2022); (Mathilde Robben, 2010)
LIBS <sup>#</sup>	1064 nm pulsed laser @ 120mJ	No	Yes	2 m/s	95 - 100% <sup>##</sup>	n/a	(Sormunenand Järvinen, 2021); (Zhao and Li, 2022); (Liu et al., 2019); (Huber et al., 2014); (Sattmann et al., 1998)
Raman	785 nm laser @ 4 W (focused)	No	Yes	n/a	93 - 98%	95%	(Sormunenand Järvinen, 2021); (Zhao and Li, 2022); (Tsuchida et al., 2009)
Digital watermark	Halogen lamp	Yes (watermark)	No	3 - 4.5 m/s	95.9% <sup>###</sup>	95.1% <sup>§</sup>	(HolyGrail 2.0, 2023)
Luminescent TBS	UV lamp	Yes (luminescent marker)	No	4.5 m/s	n/a	96% <sup>§§</sup>	(Kosior, 2020)
Organic dyes Ln markers	980 nm laser @ 1 W/cm <sup>2</sup>			4.5 m/s	>99.9% <sup>§§§</sup>	>97.4% <sup>§§§</sup>	(Moesslein et al., 2023)

<sup>#</sup> Only for chlorine containing polymers the sorting was performed on a conveyor belt. Other LIBS tests were performed in static conditions (Junjuri and Gundawar, 2019) (Costa et al., 2017) (Costa et al., 2017).

<sup>##</sup> Accuracy drops down to 73% in presence of additives (Peng et al., 2021).

<sup>###</sup> Reported as "Detection efficiency" for separation of labelled non-food PET vs post-consumer waste in two-pass process.

<sup>§</sup> Reported as "Sorting efficiency" for labelled non-food PET vs post-consumer waste for separation of labelled non-food PET vs post-consumer waste in two-pass process.

<sup>§§</sup> For PET.

<sup>§§§</sup> In two-pass industrial sorting of PE food-grade multilayer packaging. The purity of 97.4% was achieved with an atypical large amount of agricultural foils in the waste due to the French origin of the waste. If the mass of these large foils is deducted, the purity was 99%.

Consequently, Ln<sup>3+</sup>-doped markers exhibit a non-toxic nature. As a representative example, Polysecure GmbH has been able to achieve and declare compliance with European regulations for plastic materials in contact with food for an oxysulfide-based marker, after thorough migration, toxicological and other tests by independent laboratories. In addition, food contact approval is expected from the U.S. Food and Drug Administration (FDA).

To compare the difference between using an organic dye or an inorganic phosphor for tracer-based sorting, one must first consider the huge difference in absorption cross-section between an organic dye - Lumogen Red ( $8 \times 10^{-17} \text{ cm}^2$  @ 575 nm) and the Yb<sup>3+</sup> ion ( $7 \times 10^{-21} \text{ cm}^2$  @ 978 nm). This suggests that to overcome this  $10^4$  difference, the loading of the marker in the polymer would need to be increased by a similar amount. However, this was not found to be the case. A label with a marker concentration of  $50 \mu\text{g}/\text{cm}^2$  and an area of  $2 \text{ cm}^2$  (giving  $100 \mu\text{g}$  of marker used) is sufficient to detect a clear UC-PL emission signal. In comparison, Ahmad used a concentration of 10 ppm of organic dyes (Ahmad, 2023). If it is assumed that the weight of the plastic bottle used in Ahmad's experiment is approximately 20 g,  $200 \mu\text{g}$  of dye would be needed per bottle. This eliminates all the advantages of the higher absorption cross section of organic dyes, as their quantity is required to be similar to that of the Ln<sup>3+</sup> marker. Typically, the PLQY of visible-emitting organic dyes is in the range of 50–100% (Würth et al., 2011) – indeed Lumogen Red has a 100% PQLY (Wilson and Richards, 2009) – much higher than that of UC phosphors at 3–5% (Gao et al., 2017a) (Gao et al., 2018, 2019). As noted by Ahmad (Ahmad, 2023), additives in plastics often reduce the PLQY of the dyes, thus requiring higher dye concentrations (> 10 ppm). Moreover, the PLQY of Ln<sup>3+</sup> ions can be greatly increased when using the DS emission in the NIR, where PLQY values of up to 70% have been reported (Rajagopalan et al., 2023) that altogether demonstrate advantage of using Ln<sup>3+</sup> markers.

The market price for both organic dyes and Ln<sup>3+</sup> materials can fluctuate. However, if the price each is considered – e.g. 12,68 €/kg for Yb<sub>2</sub>O<sub>3</sub> (Institute for Rare Earths and Metals AG, 2024) and a well-known commercial luminescent dye such as Lumogen Red (synonyms: Perylene Red, Fluorescent Red), which costs 60 €/g (Kremer Pigmente GmbH) – the difference in material cost becomes an additional winning aspect for Ln<sup>3+</sup>-based markers. In addition, the InGaAs detector of a modern sorting machine is not sensitive enough in the visible range, where most organic dyes emit light. Considering the price of dyes emitting in the NIR

range, they are much more expensive (they cannot currently be produced on a kg scale) and their PLQY is significantly lower. Taking into account all the advantages of Ln<sup>3+</sup> ions as luminescent markers, it appears that Ln<sup>3+</sup> has a clear potential in plastics sorting applications based on luminescence detection.

Depending on the choice of host material, after excitation at 980 nm either an upconversion (UC) signal in the visible/NIR or downshifted (DS) emission in the NIR (1000 – 1800 nm) can be observed (see Fig. 2). Both processes have the advantage over other luminescent markers that their signals are background free. There is no autofluorescence from the plastic in either case. For the UC scenario, the unique energy level structure present in the lanthanides that enables anti-Stokes UC process is not present in normal materials such as plastics. For NIR DS emission, the probability of emission becomes highly inefficient in organic materials at wavelengths longer than 900 nm due to fast non-radiative relaxation between the close-lying energy levels, thus only the DS emission from the lanthanide marker remain. The 980 nm excitation is amenable to excitation with powerful and inexpensive diode lasers. Furthermore, the UC and NIR DS emission is easily observable with standard hyperspectral detectors used in sorting applications, with the NIR emission even observable concurrently with an NIR reflectance measurement.

The industrial application of UC markers for plastic sorting has been discussed in previous work (Woidasky et al., 2020; Gasde et al., 2021). The novelty of this work is that, beyond demonstrating how many upconversion codes can be uniquely identified, it is shown that down-shifted emission can be measured. The down-shifted emission opens the possibility of adding new codes, and this downshifted emission can even be measured at the same time as diffuse NIR reflectance. The industrial applicability is shown in the example that food-grade PET recycle is usually at least €300 per tonne more valuable than non-food grade PET recycle (Kahlert and Bening, 2022). By allowing the plastic packaging waste stream to be sorted into more fractions than currently possible, like distinct fractions of food-grade and non-food-grade PET photonic markers could increase the average value of sorted bales produced at a materials recovery facility, and allow true circularity in plastic packaging to be approached. Lanthanide based photonic markers have reached Technology readiness level (TRL) 6 (technology demonstrated in relevant environment) when considering binary marked/non-marked decision making in plastics packaging (Circular

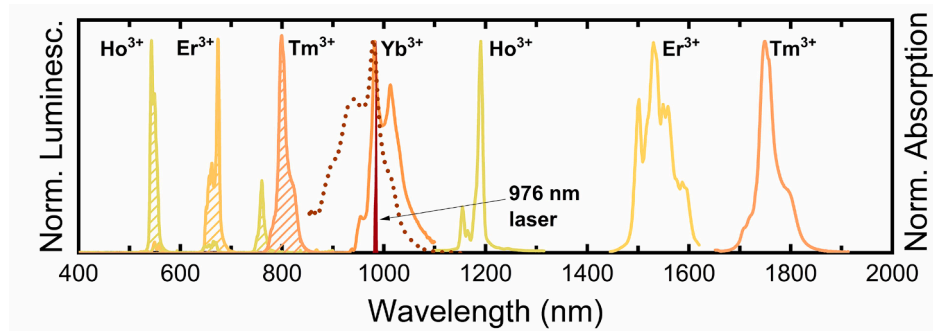


**Fig. 2.** The absorption of the  $\text{Yb}^{3+}$  sensitizer, upon which most current lanthanide photonic markers are based, is shown in the dashed line. When the broad  $\text{Yb}^{3+}$  absorption peak is excited by a 976 nm laser, different luminescence is observed depending on the host and co-doped emitter ions. Luminescent markers activated with holmium ( $\text{Ho}^{3+}$ ) exhibit UC (maximum at 543 nm) or DS (maximum at 1190 nm) luminescence. When activated with erbium ( $\text{Er}^{3+}$ ), UC (maximum at 674 nm) or DS (maximum at 1530 nm) luminescence is observed. Similarly, when activated with thulium ( $\text{Tm}^{3+}$ ), UC (maximum at 798 nm) or DS (maximum at 1750 nm) luminescence can be seen. Finally, when sensitised with  $\text{Yb}^{3+}$  alone, DS (maximum at 982 nm) luminescence is observed.

Foodpack, 2022).

Furthermore, from an industrial application perspective, fluorescent markers are particularly attractive in conjunction with shielded, laser-safe detectors which allow the use of strong excitation fields. These in turn enable reliable fluorescent signals at low marker concentrations. Such shielded detectors are possible with the patented SORT4CIRCLE technology (Polysecure GmbH, 2024) which employs singulation and subsequent single-step sorting. In addition, single-step sorting provides for each object the efficient sequential measurement of NIR reflection, colour, watermark and marker. For the first time, the simple use of all relevant detection technologies creates a technology-open sorting process that eliminates the need for the tedious and practically impossible coordination of sorting standards. Another application advantage of fluorescent markers and single-step sorting is that all fractions could be defined and sorted in one process step according to their most efficient subsequent recycling pathway. So further sorting at later stages can be reduced or even omitted.

Thanks to these scientific and technical benefits, it is apparent that fluorescent markers and single-step sorting would not increase the costs of plastic recycling, but instead improve the quality and rate of recycling greatly. Based on developments in recent years in the field of markers, detectors and sorting machine construction, the sorting cost outlook for single-step sorting with markers has been reduced to the range of €100 - 200 per tonne of throughput. Marker costs are in the range of €20 - 50 per tonne of packaging material today (or €2 - 5 per gram of marker). Importantly, single-step sorting costs almost do not grow with an increasing number of sorting fractions, in contrast to the step-wise sorting of today. Economically, this factor is essential since a real circular economy and the concept of closed loops require a larger number of sorted fractions. Based on these technical and economical improvements, fluorescent markers and single-step sorting would accelerate the advent of a real circular economy of plastics.

Regarding the size of an industrial application, the world currently produces around 300 million tonnes of plastic waste each year, and the trend is rising. For practically all waste streams single-stage sorting with markers would be an improvement against the existing stepwise sorting or no sorting. In this respect, the application potential of markers and single-stage sorting technology is over 100 million tonnes per year and therefore over 10 billion euros in turnover per year.

## 2. Experimental part

Luminescent markers used in the current work are inorganic microcrystalline materials. Typical examples of these hosts are  $\text{Gd}_2\text{O}_3$ ,  $\text{La}_2\text{O}_3$  and  $\text{Li}_3\text{Ba}_2\text{Gd}_3(\text{MoO}_4)_8$ , all of which can be co-doped with  $\text{Yb}^{3+}$ ,  $\text{Yb}^{3+}/\text{Er}^{3+}$ ,  $\text{Yb}^{3+}/\text{Ho}^{3+}$  or  $\text{Yb}^{3+}/\text{Tm}^{3+}$ . The strength of the luminescence signal from lanthanide ions is strongly dependant on the origin of the

inorganic host and the doping concentration, so it is often necessary to investigate many hosts and many doping concentrations in order to find markers with the strongest luminescence for each lanthanide ion ( $\text{Yb}^{3+}$ ,  $\text{Er}^{3+}$ ,  $\text{Ho}^{3+}$  and  $\text{Tm}^{3+}$ ). Luminescent markers were synthesised using a high temperature solid state reaction (a representative example is presented in Fig. 3a). Raw materials (typically oxides) are mixed in a stoichiometric ratio and calcined in alumina crucibles at elevated temperature (typical range 800 - 1200 °C) for several hours, with subsequent purification and drying. After synthesis, the crystal structure (and phase purity), microcrystal size and chemical composition are confirmed by powder X-ray diffraction (Bruker, D8 Discover), scanning electron microscopy (Zeiss, Supra 60VP) as illustrated in Fig. 3. Elemental analysis was performed with wavelength dispersive X-ray fluorescence spectroscopy (Bruker AXS, Pioneer S4). Other representative examples of the synthesis and characterisation of the above markers can be found in past publications from the present authors (Gao et al., 2017b) (Gao et al., 2019) (Rajagopalan et al., 2023). The photoluminescence quantum yield (PLQY, ratio of emitted photons to absorbed photons) was determined experimentally for each marker by employing an integrating sphere (Madirov et al., 2023). This approach served as a robust figure of merit, facilitating the comparison of luminescence signal strength across different markers. In the case of UC markers, PLQY fell within the range of 2–4% (Gao et al., 2019). Conversely, for DS markers, the PLQY exhibited significantly higher values, reaching up to 70% for  $\text{Li}_3\text{Ba}_2\text{Gd}_3(\text{MoO}_4)_8:\text{Yb}^{3+},\text{Er}^{3+}$  marker (Rajagopalan et al., 2023).

The absorption spectrum is detected with an UV–visible-NIR spectrophotometer (Agilent, Cary 7000) equipped with an integrating sphere in absorbance mode. The visible emission spectra of all studied samples are obtained with a spectrometer (Ocean Insight, QEPro, 300 – 1100 nm). The NIR emission spectra of the samples doped with  $\text{Yb}^{3+}$  and  $\text{Er}^{3+}/\text{Yb}^{3+}$  is obtained with a NIR spectrometer (Ocean Insight, NIR-Quest, 900–1650 nm). The NIR emission spectra of the samples doped with  $\text{Ho}^{3+}/\text{Yb}^{3+}$  and  $\text{Tm}^{3+}/\text{Yb}^{3+}$  are obtained with an extended NIR spectrometer (Zeiss, PGS NIR 2.2–256, 1000–2150 nm). A 976 nm laser diode (Roithner) driven by a laser diode controller (ITC4001, Thorlabs) is used as the excitation source.

For determining the upconversion codes, excitation is provided by a 980 nm fibre-coupled laser and the upconverted emission is measured by three Si-based detectors with appropriate band-pass filters to capture the upconversion in the green, red, and NIR spectral windows. The code is related to the fraction of the total marker material in the sample that is doped by holmium ( $\text{Ho}^{3+}$ ), erbium ( $\text{Er}^{3+}$ ), and thulium ( $\text{Tm}^{3+}$ ), which add up to 100%. As the pure markers have some overlap in emission, first the fraction of the total emission in each of the three spectral windows is computed, then least squares fit is used to best estimate the fraction of each marker material (based on the known spectra of the pure

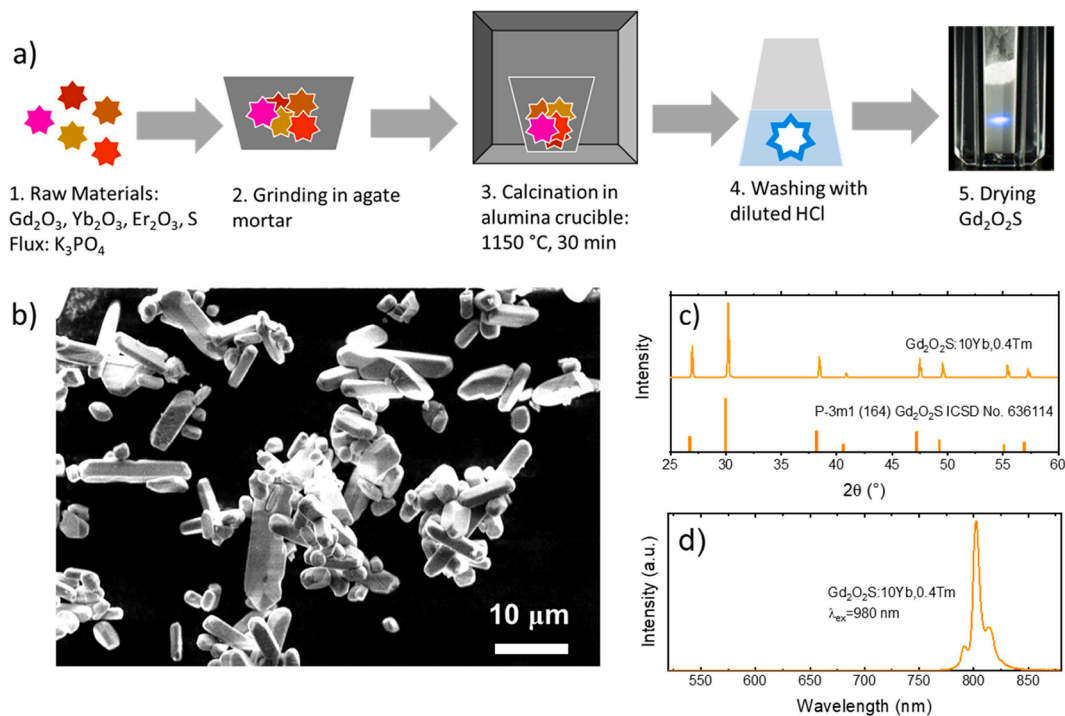


**Fig. 3.** (a) Schematic of a solid-state reaction in which raw materials are ground, subjected to high-temperature calcination, purified and dried, resulting in a microcrystalline marker  $\text{Gd}_2\text{O}_2\text{S}:\text{Yb},\text{Tm}$  that exhibits NIR and blue (visible) luminescence when excited by a 980 nm laser; (b) SEM image of a representative marker; (c) pXRD of representative marker; (d) Luminescent spectrum of a representative marker under 980 nm laser excitation. Marker -  $\text{Gd}_2\text{O}_2\text{S}$  co-doped with  $\text{Yb}^{3+}$  and  $\text{Tm}^{3+}$ .

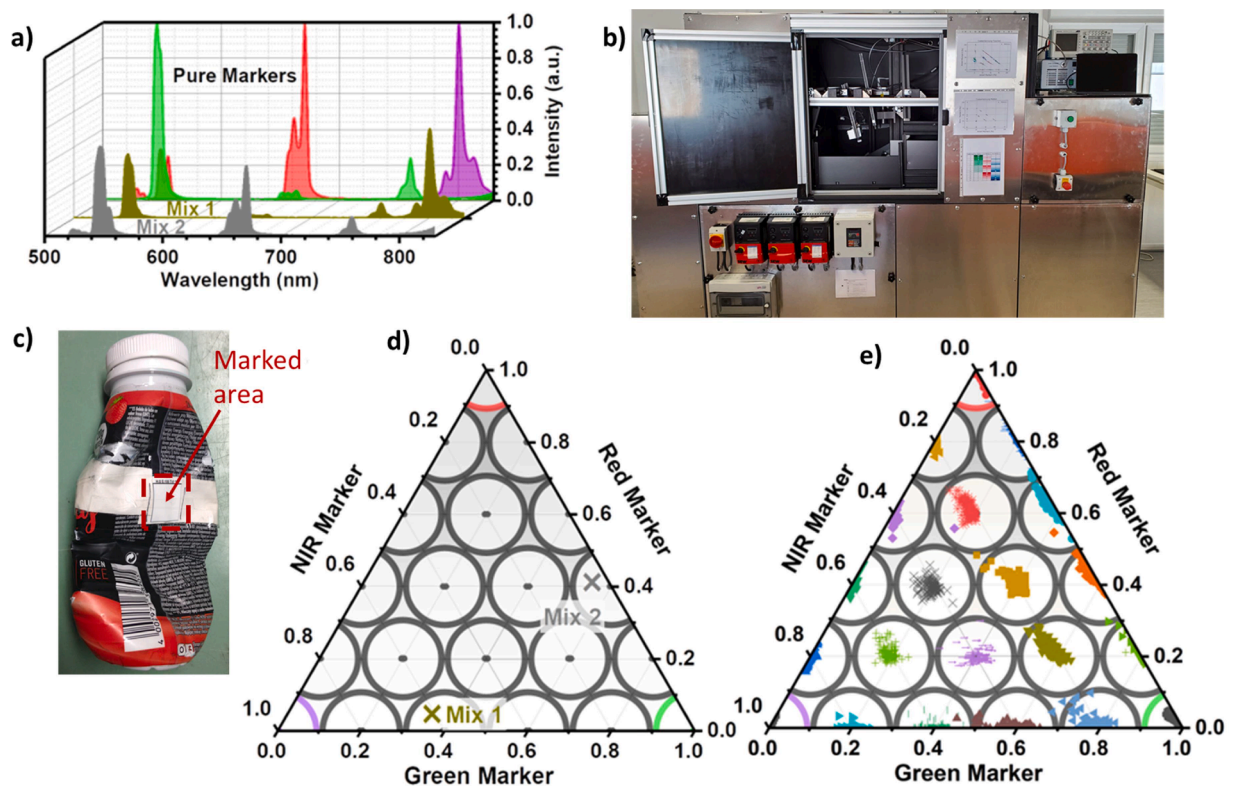


**Fig. 4.** a) Emission spectra of pure green, red, and NIR marker material, two different mixtures (Mix 1 = 40% green, 0% red, 60% NIR, Mix 2 = 60% green, 40% red, 0% NIR); b) Photograph of a machine consisting of a conveyor belt, a 980 nm excitation laser and an optical detection unit; c) Photograph of a sample (contaminated and crumpled plastic bottle) bearing a sticker (marked area) with a luminescent marker (concentration  $50 \mu\text{g}/\text{cm}^2$ ); d) Ternary diagram indicating the central points for 21 codes equidistantly spaced in terms of percentage of each marker along with examples of positions for the pure markers and two mixes shown in panel a; e) Results of 2100 runs of discs labelled with each of the 21 codes in a prototype sorting machine. The system functions with 99% accuracy.

marker materials). The markers were applied to plastic PET bottles using a white sticker with a marker concentration of  $50 \mu\text{g}/\text{cm}^2$  (Fig. 4c). A conveyor belt (3 m/s) was loaded with plastic bottles, which were irradiated with a 100 W 980 nm laser (CNI Laser, FC-W-980H) inside the machine (Fig. 4b). The UC luminescence was detected using 3 Si-diodes (Ketek, SIPM3315) equipped with appropriate optical filters (Semrock) to detect green, red and NIR luminescence.

The classification of the plastic materials in the range of 1100 – 2100 nm was performed with a hyperspectral camera operating in the NIR region (Specim, FX17). The sample is illuminated with two light sources – a 150 W halogen lamp (Elro, HL150) and a 980 nm fibre laser (CNI Laser, FC-W-980H) with an intensity of  $3.3 \text{ W}/\text{cm}^2$ . Reflectance spectra are obtained using the reference spectrum of a white calibration tile (Specim, OPRS 200.25.10).

### 3. Results and discussion

#### 3.1. Upconversion: three-colour codes in the visible

As illustrated in Fig. 2 above,  $\text{Ho}^{3+}$ ,  $\text{Er}^{3+}$ , and  $\text{Tm}^{3+}$  emitter ions can give relatively pure green ( $\text{Ho}^{3+}$ ), red ( $\text{Er}^{3+}$ ) and 798 nm NIR ( $\text{Tm}^{3+}$ ) UC emission after excitation at 940 or 976 nm (when co-doped with  $\text{Yb}^{3+}$  as the light-absorbing sensitizer ion). Fig. 4a and 4b present photographs of the UC from the microcrystalline powders after excitation with 940 nm LEDs in a dark and light ambient environment, respectively. The strong visible emission of  $\text{Ho}^{3+}$  and  $\text{Er}^{3+}$  is easily observed, and the invisible 798 nm radiation of  $\text{Tm}^{3+}$  appears purple in the camera image due to some breakthrough of the NIR radiation through the NIR and Bayer colour filters.

An important question is how many classes can be precisely identified when mixtures of these three materials are used to create a coding system? Firstly, the coding system on which classification is based depends on the detection system that is used. One option for a coding system that is to simply examine the intensity in three spectral regions, e.g., 525–575 nm, 640–690 nm, and 775–825 nm, as presented in Fig. 2. To make a classification, the percentage of the total observed signal from each of the channels is computed, then this is converted into the percentage of each marker present. This metric has two degrees of freedom – as the total signal is normalised to 100% it is possible to compute amount of the third marker if the fractions of the other two markers are known. An example of the total emission spectrum of the pure markers compared the normalised emission for a two different mixes of different marker types can be found in Fig. 4c.

A ternary diagram is useful for visualizing the possible outcomes of a measurement, where the three sides of the triangle represent the fraction of the total concentration of each marker. An idealised example of such a ternary diagram is shown in Fig. 4d, demonstrating how 21 unique codes could be created by spacing the “target” percentages in 20% steps on each marker axis. The grey dots represent the targeted concentration profile for each of the 21 unique codes, and grey circles represent the area in which a measured point would be assigned to code corresponding to the circles’ centre. The circles for the cases in which 100% of the emission comes from the  $\text{Tm}^{3+}$ ,  $\text{Er}^{3+}$ , or  $\text{Ho}^{3+}$  are indicated in purple, red, and green, respectively. Although the  $\text{Ho}^{3+}$  and  $\text{Er}^{3+}$  emissions overlap ( $\text{Ho}^{3+}$  is not a purely green marker, with roughly 10% of its emission lands in the red channel, and likewise around 10% of the  $\text{Er}^{3+}$  ends up in the green channel), the system of four equations (three colour channels plus the normalisation) with three variables yields a unique solution for the fraction of each marker varying from 0 to 100%.

A ternary diagram showing the measured locations of the marker codes for 2100 measurements, 100 for each code is presented in Fig. 4e. The estimation of the code location on the ternary diagram has some scatter but less than 20 of the 2100 measurements led to the inability to assign a code or a false code assignment. The accuracy is therefore greater than 99%. With developments in optical design, it should be possible to increase this accuracy even more.

To increase the number of useable codes two options would be to increase the number of emission lines (i.e., increase the number of marker materials) or the precision with which the components can be measured. The number of codes,  $N$ , can be expressed in terms of emission lines,  $n$ , and the step size in concentration between the centre of two codes difference in concentration,  $l$  (in Fig. 2b this is 20%). The number of codes obtainable is  $N = \binom{n+l-1}{n}$  and Table 3 below shows how

the number of unique codes increases with number of emission lines available to make the code, and step size in concentration. It is clear that adding new lines expands the code space. Furthermore, decreasing the scatter in measurements would allow smaller changes in concentration between the centre of codes, and more codes to be fit into the same space. In the past, there have been many reports of UC luminescence with  $\text{Pr}^{3+}$  (Gao et al., 2014),  $\text{Eu}^{3+}$  (Wang et al., 2008) and  $\text{Tb}^{3+}$  (Xiao et al., 2017),  $\text{Sm}^{2+}$  (Liu et al., 2017) using sensitisation with  $\text{Yb}^{3+}$ . However, it seems impossible to achieve their UC luminescence with PLQY similar to that of  $\text{Er}^{3+}$ ,  $\text{Ho}^{3+}$  and  $\text{Tm}^{3+}$  at excitation intensity below  $\sim 10 \text{ W}/\text{cm}^2$ . Therefore, additional attention should be paid to the NIR spectral region where, in addition to  $\text{Er}^{3+}$ ,  $\text{Ho}^{3+}$  and  $\text{Tm}^{3+}$ , strong emission from  $\text{Pr}^{3+}$  (Wang et al., 2023) and some transition metals such as  $\text{Ni}^{2+}$  and  $\text{Cr}^{4+}$  (Rajendran et al., 2023) could be expected.

Looking at the other option to gain more codes, decreasing the minimum step size in weight% in the coding system, the approached would be continuing to engineer the excitation and detection system to measure the emission with increased signal to noise ratio.

#### 3.2. Combination of NIR emission and NIR reflectance

A few NIR sorters include an extended NIR spectrometer to cover the 1100 – 1800 nm range. These machines could be used to detect and sort new packaging waste fractions by NIR emission lines of luminescent markers. and likewise exploit another attractive aspect of lanthanide luminescent markers, namely that, in the correct hosts, they can exhibit strong and distinct emission in the NIR. By co-doping with  $\text{Yb}^{3+}$  these transitions can be effectively stimulated by LED or laser excitation in the region 940 to 980 nm. For  $\text{Ho}^{3+}$ ,  $\text{Er}^{3+}$  and  $\text{Tm}^{3+}$  this is illustrated in Fig. 2 where strong emission lines are shown around 1190, 1530 and 1790 nm respectively. Like the UC example shown in the previous section, the DS luminescence in the NIR region can provide a high-contrast, background-free signal as emission from organics in this wavelength range is very inefficient.

To visualise this emission, cuvettes filled with micro powders wherein  $\text{Ho}^{3+}$ ,  $\text{Er}^{3+}$ , and  $\text{Tm}^{3+}$  are co-doped with  $\text{Yb}^{3+}$  were placed beside a  $\text{Yb}^{3+}$  only doped sample underneath an extended InGaAs hyperspectral camera (Specim NIR, 1000 – 2500 nm). In Fig. 5a, an image of the cuvettes is shown when the powders are excited by the array of 940 nm LEDs and there is no other ambient light. The false colour image is generated from the hyperspectral cube by taking the blue channel to be the intensity at 1800 nm, the red channel to be the emission at 1550 nm, and the green channel at 1180 nm. In this case only the three cuvettes with emission above 1150 nm are visible, where the  $\text{Tm}^{3+}$ ,  $\text{Er}^{3+}$ , and  $\text{Ho}^{3+}$  provide emission at these wavelengths, respectively. In Fig. 5b, a halogen light bar is also used to illuminate the sample at the same time as the 940 nm LED excitation. In this case, the

**Table 3**

Number of unique codes available as a function of the number of unique emission lines and the step size between component weights that can still be accurately classified.

Step Size	10%	20%
Number of unique emission lines		
3	66	21
4	286	56
5	1001	126

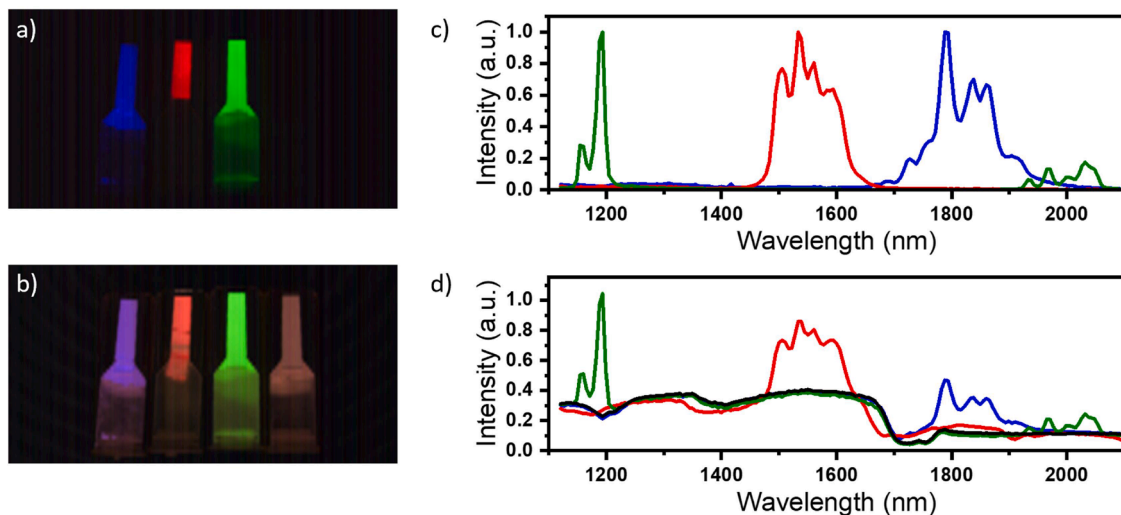


**Fig. 5.** NIR hyperspectral data collected for downshifting markers in PMMA cuvettes under 940 nm LED excitation only (a,c) or concurrent excitation with the LEDs and a halogen light bar to enable concurrent measurement of diffuse reflectance (b,d). a-b) show false colour images of the four cuvettes filled with powder with the red, green, and blue channels representing the intensity at 1550, 1800, and 1180 nm. From right to left the materials are  $\text{Tm}^{3+}$ ,  $\text{Er}^{3+}$ , and  $\text{Ho}^{3+}$  co-doped with  $\text{Yb}^{3+}$ , then a reference doped solely with  $\text{Yb}^{3+}$  (not visible in a). c-d) The emission spectra at representative pixels for each material recorded by the hyperspectral camera. The green, red, and blue lines indicate the  $\text{Ho}^{3+}$ ,  $\text{Er}^{3+}$ , and  $\text{Tm}^{3+}$  emissions respectively, whereas the black line in d) indicates the diffuse reflectance from the reference powder registering the absorption lines of the cuvette's polymer. As in c), clear emissions of the markers are observable in d) even on top of the intense broadband light from the halogen lamps that also carries the signature of the polymer's absorption.

diffuse reflectance of the broadband halogen illumination causes the reference powder to become visible and appear whitish in the false colour image. The colour saturation of the marker materials is also reduced by their diffuse reflectance, but nonetheless the different nature of the markers is still clearly distinguishable in the false colour images, meaning that even in the presence of broadband illumination to enable material classification through diffuse reflectance, the markers can still be measured. Example spectra measured at single pixels in the relevant regions of interest in the hyperspectral cube are shown for 940 nm LED excitation only in Fig. 5c and illumination with the halogen light bar in addition to the 940 nm excitation in Fig. 5d. In Fig. 5c, each emission profile of the three markers provides a clean background-free signal. These three high-contrast signals provide a basis upon which a coding system could be built (such as the one introduced in the preceding section). In panel d) the broadband diffuse reflectance of the halogen light spectra can be seen in the diffuse reflectance spectra of the reference  $\text{Yb}^{3+}$  only doped powder shown as the black line. The dips in reflection around 1200 nm and 1720 nm are typical of the polymethylmethacrylate (PMMA) polymer from which the cuvette is made. When the DS lanthanides are co-doped with the  $\text{Yb}^{3+}$ , the NIR emission lines become clearly visible on top of the diffuse reflectance of the halogen lighting, with the light collected at emission peaks exceeding that of the diffuse reflection. Thus, there is excellent perspective for lanthanides to provide NIR emission lines that could also provide the basis for a background free coding system for plastic sorting, with further work to increase the number of lines available while maximising their efficiency and stability of great interest.

#### 4. Conclusions

This work discusses how nuanced sorting of plastic post-consumer packaging waste is likely to be a keystone for further development of a plastics recycling ecosystem that supports the move towards circularity. For this a code-based system that does not disturb products appearance to consumers but is easily recognised in sorting facilities is of clear interest. This article elaborates on how luminescent lanthanide markers can contribute solutions to generate such a coding system. Upconversion markers with emission in the visible can certainly be used, with the upconversion luminescence providing a background free signal.

For example, mixes of three different UC powders could be used to make 21 different codes that were recognised with >99% accuracy. Looking to the future, this code space could be enhanced by the addition of further emission spectra, or an increase in the precision with which the codes can be read. Another promising perspective is the use of DS emitters to develop an equivalent coding system in the NIR. Such a coding system could possibly be read out by the same detector that measures the diffuse reflectance of the unmarked parts of the plastic object. Lanthanide based luminescent markers are an excellent candidate for providing a code system that satisfies the above requirements, providing new perspectives for phosphor and sorting machine development.

#### CRediT authorship contribution statement

**Ian A. Howard:** Conceptualization, Data curation, Formal analysis, Writing – original draft, Writing – review & editing. **Dmitry Busko:** Formal analysis, Investigation, Methodology. **Guojun Gao:** Formal analysis, Investigation, Methodology, Validation, Visualization. **Pascal Wendler:** Data curation, Formal analysis, Investigation, Methodology, Validation, Visualization. **Eduard Madirov:** Formal analysis, Investigation, Methodology, Validation, Visualization. **Andrey Turshatov:** . **Jochen Moesslein:** Funding acquisition, Project administration, Resources, Supervision, Writing – review & editing. **Bryce S. Richards:** Conceptualization, Data curation, Funding acquisition, Project administration, Resources, Supervision, Writing – original draft, Writing – review & editing.

#### Declaration of competing interest

The authors declare the following financial interests/personal relationships which may be considered as potential competing interests: Bryce S. Richards reports financial support was provided by Helmholtz Association of German Research Centres. Bryce S. Richards reports financial support was provided by Horizon 2020 European Innovation Council Fast Track to Innovation. If there are other authors, they declare that they have no known competing financial interests or personal relationships that could have appeared to influence the work reported in this paper.

## Data availability

Data will be made available on request.

## Acknowledgements

The financial support provided by the Helmholtz Association is gratefully acknowledged: (i) a Recruitment Initiative Fellowship for B.S. R.; (ii) the funding of chemical synthesis equipment from the Helmholtz Materials Energy Foundry (HEMF); and (iii) Research Field Energy – Program Materials and Technologies for the Energy Transition – Topic 1 Photovoltaics. B.S.R. and A.T. acknowledge funding from the European Union’s Horizon 2020 research and innovation project “Circular Food-pack” agreement No: 101003806.

## References

- Ahmad, S.R., 2023. Tracer technology in plastic identification—Past, present and future. *Nanotechnol. Percept.* 19, 27–40. <https://doi.org/10.4024/N07AH22A.ntp.19.01>.
- Anuar Sharuddin, S.D., Abnisa, F., Wan Daud, W.M.A., Aroua, M.K., 2016. A review on pyrolysis of plastic wastes. *Energy Convers. Manage* 115, 308–326. <https://doi.org/10.1016/j.enconman.2016.02.037>.
- Brunner, S., Fomin, P., Kargel, C., 2015. Automated sorting of polymer flakes: fluorescence labeling and development of a measurement system prototype. *Waste Manage.* 38, 49–60. <https://doi.org/10.1016/j.wasman.2014.12.006>.
- Circular Foodpack, 2022. Milestone achieved: Successful sorting Trials With Tracer-Based-Sorting Technology. <https://www.circular-foodpack.eu/news/important-milestone-achieved-successful-sorting-trials-with-tracer-based-sorting-technology/>. Accessed 30.01.2024.
- Coates, G.W., Getzler, Y.D.Y.L., 2020. Chemical recycling to monomer for an ideal, circular polymer economy. *Nat. Rev. Mater.* 5 (7), 501–516. <https://doi.org/10.1038/s41578-020-0190-4>.
- Costa, V.C., Aquino, F.W.B., Paranhos, C.M., Pereira-Filho, E.R., 2017. Identification and classification of polymer e-waste using laser-induced breakdown spectroscopy (LIBS) and chemometric tools. *Polym. Test.* 59, 390–395. <https://doi.org/10.1016/j.polymertesting.2017.02.017>.
- Digimar, 2019. Pioneer Project HolyGrail. <https://vimeo.com/332020546/39583c93e0>. Accessed 30.01.2024.
- European Commission, 2017. Review of Waste Policy and Legislation. [http://ec.europa.eu/environment/waste/target\\_review.htm](http://ec.europa.eu/environment/waste/target_review.htm). Accessed 30.01.2023.
- European Parliament, 2023. Plastic Waste and Recycling in the EU: Facts and Figures. <https://www.europarl.europa.eu/news/en/headlines/society/20181212STO21610/plastic-waste-and-recycling-in-the-eu-facts-and-figures>. Accessed 30.01.2024.
- GAIA, 2021. Regulatory catalysts: Rejecting Single-Use Plastics in Asia. <https://www.no-burn.org/wp-content/uploads/GAIA-AP-Regulatory-Catalysts-Rejecting-Single-Use-Plastics-in-Asia.pdf>. Accessed 30.01.2024.
- Gao, G., Busko, D., Joseph, R., Howard, I.A., Turshatov, A., Richards, B.S., 2018. Highly Efficient La2O3:Yb3+,Tm3+ Single-Band NIR-to-NIR Upconverting Microcrystals for Anti-Counterfeiting Applications. *ACS Appl. Mater. Interfaces.* 10 (46), 39851–39859. <https://doi.org/10.1021/acsami.8b11196>.
- Gao, G., Busko, D., Joseph, R., Turshatov, A., Howard, I.A., Richards, B.S., 2019. High Quantum Yield Single-Band Green Upconversion in La2O3:Yb3+, Ho3+ Microcrystals for Anticounterfeiting and Plastic Recycling. *Part. Part. Syst. Characterization* 36 (3), 1800462. <https://doi.org/10.1002/ppsc.201800462>.
- Gao, G., Busko, D., Kauffmann-Weiss, S., Turshatov, A., Howard, I.A., Richards, B.S., 2017a. Finely-tuned NIR-to-visible up-conversion in La2O3:Yb3+,Er3+ microcrystals with high quantum yield. *J. Mater. Chem. C* 5 (42), 11010–11017. <https://doi.org/10.1039/C6TC05322J>.
- Gao, G., Turshatov, A., Howard, I.A., Busko, D., Joseph, R., Hudry, D., Richards, B.S., 2017b. Up-Conversion Fluorescent Labels for Plastic Recycling: a Review. *Adv. Sustain. Syst.* 1 (5), 1600033. <https://doi.org/10.1002/adsu.201600033>.
- Gao, W., Zheng, H., Gao, D., He, E., Li, J., Tu, Y., 2014. Pr<sup>3+</sup>/Yb<sup>3+</sup> Co-Doped b-Phase NaYF<sub>4</sub> Microprisms: controlled Synthesis and Upconversion Luminescence. *J. Nanosci. Nanotechnol.* 14 (6), 4308–4312. <https://doi.org/10.1166/jnn.2014.8042>.
- García, J.M., Robertson, M.L., 2017. The future of plastics recycling. *Science* (1979) 358 (6365), 870–872. <https://doi.org/10.1126/science.aag0324>.
- Gasde, J., Woidasky, J., Moesslein, J., Lang-Koetz, C., 2021. Plastics recycling with tracer-based-sorting: challenges of a potential radical technology. *Sustainability* 13 (1), 258. <https://doi.org/10.3390/su13010258>.
- Gontard, N., David, G., Guilbert, A., Sohn, J., 2022. Recognizing the long-term impacts of plastic particles for preventing distortion in decision-making. *Nat. Sustain.* 5 (6), 472–478. <https://doi.org/10.1038/s41893-022-00863-2>.
- HolyGrail 2.0, 2023. <https://www.packworld.com/design/package-design/article/22865876/holygrail-20-proving-viable-at-scale>. (Accessed 05.02.2024).
- Huber, N., Eschböck-Fuchs, S., Scherndl, H., Freimund, A., Heitz, J., Pedarnig, J.D., 2014. In-line measurements of chlorine containing polymers in an industrial waste sorting plant by laser-induced breakdown spectroscopy. *Appl. Surf. Sci.* 302, 280–285. <https://doi.org/10.1016/j.apsusc.2013.10.070>.
- Institute for Rare Earths and Metals AG, 2024. <https://ise-metal-quotes.com/>. (Accessed 30.01.2024).
- Jehanno, C., Alty, J.W., Roosen, M., De Meester, S., Dove, A.P., Chen, E.Y.-X., Leibfarth, F.A., Sardon, H., 2022. Critical advances and future opportunities in upcycling commodity polymers. *Nature* 603 (7903), 803–814. <https://doi.org/10.1038/s41586-021-04350-0>.
- Junjuri, R., Gundawar, M.K., 2019. Femtosecond laser-induced breakdown spectroscopy studies for the identification of plastics. *J. Anal. At. Spectrom.* 34 (8), 1683–1692. <https://doi.org/10.1039/C9JA00102F>.
- Kahlert, S., Bening, C.R., 2022. Why pledges alone will not get plastics recycled: comparing recylate production and anticipated demand. *Resources, Conserv. Recycl.* 181, 106279. <https://doi.org/10.1016/j.resconrec.2022.106279>.
- Kosior, E., 2020. New Fluorescent Tech Can Light Up Food Packaging Recycling Rates. *New fluorescent tech can light up food packaging recycling rates*. Accessed 05.02.2024.
- Kremer Pigmente GmbH, <https://www.kremer-pigmente.com/>. (Accessed 30.01.2024).
- Labels & Labeling, 2022. HolyGrail 2.0 Validates Detection Sorting Unit. <https://www.la-belsandlabeling.com/news/associations-and-events/holygrail-20-validates-detection-sorting-unit>. Accessed 30.01.2024.
- Larder, R.R., Hatton, F.L., 2023. Enabling the Polymer Circular Economy: innovations in Photoluminescent Labeling of Plastic Waste for Enhanced Sorting. *ACS Polym. Au* 3 (2), 182–201. <https://doi.org/10.1021/acspolymersau.2c00040>.
- Law, K.L., Narayan, R., 2021. Reducing environmental plastic pollution by designing polymer materials for managed end-of-life. *Nat. Rev. Mater.* 7 (2), 104–116. <https://doi.org/10.1038/s41578-021-00382-0>.
- Liu, K., Tian, D., Wang, H., Yang, G., 2019. Rapid classification of plastics by laser-induced breakdown spectroscopy (LIBS) coupled with partial least squares discrimination analysis based on variable importance (VI-PLS-DA). *Anal. Methods* 11 (9), 1174–1179. <https://doi.org/10.1039/C8AY02755B>.
- Liu, X., Aidilibike, T., Guo, J., Li, Y., Di, W., Qin, W., 2017. Upconversion luminescence of Sm<sup>2+</sup> ions. *RSC Adv.* 7 (23), 14010–14014. <https://doi.org/10.1039/C7RA00071E>.
- Madirov, E., Busko, D., Cardona, F.A., Hudry, D., Kuznetsov, S.V., Konyushkin, V.A., Nakladov, A.N., Alexandrov, A.A., Howard, I.A., Richards, B.S., Turshatov, A., 2023. Comparison of Quantum Yield of Upconversion Nanocrystals Determined by Absolute and Relative Methods. *Adv. Photonics Res.* 4 (2), 2200187. <https://doi.org/10.1002/adpr.202200187>.
- Mangold, H., von Vacano, B., 2022. The Frontier of Plastics Recycling: rethinking Waste as a Resource for High-Value Applications. *Macromol. Chem. Phys.* 223 (13), 2100488. <https://doi.org/10.1002/macp.202100488>.
- Mathilde Robben, H.W., 2010. Near-infrared Sorting for Minerals. [http://publications.rwth-aachen.de/record/119951/files/34\\_Near-infrared%20Sorting%20for%20Minerals%202010.pdf](http://publications.rwth-aachen.de/record/119951/files/34_Near-infrared%20Sorting%20for%20Minerals%202010.pdf). Accessed 05.02.2024.
- Moesslein, J., Treick, A., Watschke, L., 2023. Präzise Und Effizient Sortieren Mit SORT4CIRCLE®. [https://muellundabfall.de/download/168507/mua\\_20230305.pdf](https://muellundabfall.de/download/168507/mua_20230305.pdf). Accessed 05.02.2024.
- Neo, E.R.K., Yeo, Z., Low, J.S.C., Goodship, V., Debattista, K., 2022. A review on chemometric techniques with infrared, Raman and laser-induced breakdown spectroscopy for sorting plastic waste in the recycling industry. *Resources, Conserv. Recycl.* 180, 106217. <https://doi.org/10.1016/j.resconrec.2022.106217>.
- Nicholson, S.R., Rorrer, J.E., Singh, A., Konev, M.O., Rorrer, N.A., Carpenter, A.C., Jacobsen, A.J., Román-Leshkov, Y., Beckham, G.T., 2022. The Critical Role of Process Analysis in Chemical Recycling and Upcycling of Waste Plastics. *Annu Rev. Chem. Biomol. Eng.* 13 (1), 301–324. <https://doi.org/10.1146/annurev-chembioeng-100521-085846>.
- Niessner, N., 2022. Recycling of Plastics. In: Niessner, N. (Ed.), *Recycling of Plastics*. Hanser, pp. I–XXXIII.
- Peng, X., Xu, B., Xu, Z., Yan, X., Zhang, N., Qin, Y., Ma, Q., Li, J., Zhao, N., Zhang, Q., 2021. Accuracy improvement in plastics classification by laser-induced breakdown spectroscopy based on a residual network. *Opt. Express* 29 (21), 33269–33280. <https://doi.org/10.1364/OE.438331>.
- Picuno, C., Allassali, A., Chong, Z.K., Kuchta, K., 2021. Flows of post-consumer plastic packaging in Germany: an MFA-aided case study. *Resources, Conserv. Recycl.* 169, 105515. <https://doi.org/10.1016/j.resconrec.2021.105515>.
- Plastics Europe, 2020. Plastics – the Facts 2020: an Analysis of European plastics production, Demand and Waste Data. [https://plasticseurope.org/de/wp-content/uploads/sites/3/2021/11/Plastics\\_the\\_facts-WEB-2020\\_versionJun21\\_final.pdf](https://plasticseurope.org/de/wp-content/uploads/sites/3/2021/11/Plastics_the_facts-WEB-2020_versionJun21_final.pdf). Accessed 30.01.2024.
- Polysecure GmbH, 2024. <https://www.polysecure.eu/en/sort-reliably>. (Accessed 30.01.2024).
- Rajagopalan, K., Madirov, E., Busko, D., Howard, I.A., Richards, B.S., Swart, H.C., Turshatov, A., 2023. High Quantum Yield Shortwave Infrared Luminescent Tracers for Improved Sorting of Plastic Waste. *ACS Appl. Mater. Interfaces.* 15 (37), 43985–43993. <https://doi.org/10.1021/acsami.3c07387>.
- Rajendran, V., Huang, W.-T., Chen, K.-C., Wei, D.-H., Chang, H., Liu, R.-S., 2023. Shortwave Infrared Luminescence of Tetravalent Chromium and Divalent Nickel: phosphor Design Principles and Applications. *ACS Appl. Opt. Mater.* 1 (6), 1063–1079. <https://doi.org/10.1021/acsaom.2c00182>.
- Sattmann, R., Monch, I., Krause, H., Noll, R., Couris, S., Hatzia Apostolou, A., Mavromanolakis, A., Fotakis, C., Larrauri, E., Miguel, R., 1998. Laser-Induced Breakdown Spectroscopy for Polymer Identification. *Appl. Spectrosc.* 52 (3), 456–461.
- Schyns, Z.O.G., Shaver, M.P., 2021. Mechanical Recycling of Packaging Plastics: a Review. *Macromol. Rapid. Commun.* 42 (3), 2000415. <https://doi.org/10.1002/marc.202000415>.

- Sormunen, T., Järvinen, S., 2021. Report on the State-of-the-Art And Novel Solutions in Sorting Of Post-Consumer Plastic Packaging Waste. VTT Technical Research Centre of Finland.
- Stegmann, P., Daioglou, V., Londo, M., van Vuuren, D.P., Junginger, M., 2022. Plastic futures and their CO<sub>2</sub> emissions. *Nature* 612 (7939), 272–276. <https://doi.org/10.1038/s41586-022-05422-5>.
- Taneeapanichskul, N., Purkiss, D., Miodownik, M., 2022. A Review of Sorting and Separating Technologies Suitable for Compostable and Biodegradable Plastic Packaging. *Front. Sustainability* 3. <https://doi.org/10.3389/frsus.2022.901885>.
- Tsuchida, A., Kawazumi, H., Kazuyoshi, A., Yasuo, T., 2009. Identification of Shredded Plastics in milliseconds using Raman spectroscopy for recycling. In: *SENSORS, 2009 IEEE*, pp. 1473–1476. <https://doi.org/10.1109/ICSENS.2009.5398454>.
- Uekert, T., Singh, A., DesVeaux, J.S., Ghosh, T., Bhatt, A., Yadav, G., Afzal, S., Walzberg, J., Knauer, K.M., Nicholson, S.R., Beckham, G.T., Carpenter, A.C., 2023. Technical, Economic, and Environmental Comparison of Closed-Loop Recycling Technologies for Common Plastics. *ACS Sustain. Chem. Eng.* 11 (3), 965–978. <https://doi.org/10.1021/acssuschemeng.2c05497>.
- Government, U.S., 2022. Fact sheet: U.S. Actions to Address Plastic Pollution. <https://www.state.gov/u-s-actions-to-address-plastic-pollution/>. Accessed 30.01 2024.
- Wang, H., Duan, C.-k., Tanner, P.A., 2008. Visible Upconversion Luminescence from Y<sub>2</sub>O<sub>3</sub>:Eu<sup>3+</sup>, Yb<sup>3+</sup>. *J. Phys. Chem. C* 112 (42), 16651–16654. <https://doi.org/10.1021/jp8046505>.
- Wang, W., Xue, Y., Dong, J., Zhang, C., Liu, J., Hou, W., Wang, Q., Xu, X., Tang, H., Lin, H., Li, D., Wang, Z., Xu, J., 2023. Yb<sup>3+</sup>; sensitization effect to Pr<sup>3+</sup>; originated from <sup>1</sup>G<sub>4</sub> level broadband near-infrared emission and up-conversion in BaF<sub>2</sub> crystal. *Opt. Mater. Express* 13 (5), 1267–1277. <https://doi.org/10.1364/OME.471546>.
- Wilson, L.R., Richards, B.S., 2009. Measurement method for photoluminescent quantum yields of fluorescent organic dyes in polymethyl methacrylate for luminescent solar concentrators. *Appl. Opt.* 48 (2), 212–220. <https://doi.org/10.1364/AO.48.000212>.
- Woidasky, J., Sander, I., Schau, A., Moesslein, J., Wendler, P., Wacker, D., Gao, G., Kirchenbauer, D., Kumar, V., Busko, D., Howard, I.A., Richards, B.S., Turshatov, A., Wiethoff, S., Lang-Koetz, C., 2020. Inorganic fluorescent marker materials for identification of post-consumer plastic packaging. *Resources, Conserv. Recycl.* 161, 104976. <https://doi.org/10.1016/j.resconrec.2020.104976>.
- Würth, C., Grabolle, M., Pauli, J., Spieles, M., Resch-Genger, U., 2011. Comparison of Methods and Achievable Uncertainties for the Relative and Absolute Measurement of Photoluminescence Quantum Yields. *Anal. Chem.* 83 (9), 3431–3439. <https://doi.org/10.1021/ac2000303>.
- Xiao, W., Wu, D., Zhang, L., Zhang, X., Hao, Z., Pan, G.-H., Zhao, H., Zhang, L., Zhang, J., 2017. Cooperative Upconversion Luminescence Properties of Yb<sup>3+</sup> and Tb<sup>3+</sup> Heavily Codoped Silicate Garnet Obtained by Multiple Chemical Unit Cosubstitution. *J. Phys. Chem. C* 121 (5), 2998–3006. <https://doi.org/10.1021/acs.jpcc.6b11633>.
- Zhao, Y., Li, J., 2022. Sensor-based technologies in effective solid waste sorting: successful applications, sensor combination, and future directions. *Environ. Sci. Technol.* 56 (24), 17531–17544. <https://doi.org/10.1021/acs.est.2c05874>.